UNIVERSITY OF CALIFORNIA

SANTA CRUZ

EVAPORITIC CARBONATES RECORD SURFACE MELTING IN ANTARCTICA

A thesis submitted in partial satisfaction
of the requirements for the degree of

MASTER OF SCIENCE

in

EARTH SCIENCES

by

Noah Brigham

August 2026

The Thesis of Noah Brigham
is approved:

Professor Terrence Blackburn, Chair

Professor Slawomir Tulaczyk

Professor Tamara Pico

Donald Smith, Interim Vice Provost and
Dean of Graduate Studies

Table of Contents

List of Tables iv

List of Figures iv

Abstract v

1. Introduction 1

2. Materials and Methods 6

2.1 U-Th Isotopic Data..... 6

2.2 Carbon, Oxygen, and Strontium Isotopic Data..... 8

3. Results 9

4. Discussion 12

4.1 Constraints from Carbon and Oxygen Data 12

4.2 Constraints from Strontium Isotopic Data 14

4.3 Timing of Carbonate Formation 15

4.4 Surface Melting Radiative Balance..... 20

5. Conclusion 22

References 25

List of Tables

Table 1. Summary of U-Th isotopic data 11

Table 2. Summary of carbon, oxygen, and strontium isotopic data, and other relevant sample information 12

List of Figures

Figure 1. Regional map of the Ross Sea Sector showing sample locations and a sample photo 5

Figure 2. Sample photo of PRR_33067 6

Figure 3. Rosholt A Isochron for PRR_33067..... 8

Figure 4. Scatter plot of Carbon and oxygen compositions 14

Figure 5. Timeseries stack with U-Th carbonate ages 19

Figure 6. Surface melting radiative balance model results..... 22

Abstract

Evaporitic carbonates record surface melting in Antarctica

Noah Brigham

Changes in Pleistocene Antarctic temperatures often coincide with variations in Northern Hemisphere summer insolation. While models invoking global CO_2 changes and shifts in oceanic and atmospheric circulation explain the temperature coherence between the poles, the role of Southern Hemisphere insolation in local Antarctic temperatures remain unclear. Here we present a temporal and geochemical record of Antarctic surface melting recorded by evaporitic carbonate formation from eight sites spanning the Amundsen Sea to the Ross Sea and 365m - 2000m in elevation. Isotopic data indicate water sourced from surface melt that weathers local rock and saturates carbonate through evaporation. U–Th dates restrict carbonate formation to three of the five most recent periods of high Southern Hemisphere summer insolation. These observations calibrate the effective albedo of darkened surfaces near nunataks and identify a Southern Hemisphere summer insolation threshold at which surface melt can occur under polar conditions.

1. Introduction

Calcium carbonate (calcite) ($CaCO_3$) is a common mineral that forms encrustations in a wide range of environments including desert soils and polar environments (Zamanian et al., 2016). In polar regions, crusts or rinds of calcium carbonate mineralization commonly coat the underside of moraine clasts or exposed rock surfaces and have been well studied in the Arctic and alpine regions of Europe (Lacelle, 2007; Lacelle et al., 2007). Their occurrence on silicate bedrock has been interpreted to result from surface waters actively weathering silicate rocks while their isotopically high $\delta^{13}C$ and $\delta^{18}O$ values have been interpreted as kinetic fractionation resulting from the evaporation of water that drives calcite saturation and precipitation (Lacelle, 2007). Both observations, therefore, imply the presence of surface waters occurring in polar regions. There is also widespread occurrence of these carbonate crusts in Antarctica, with previously studied examples in the Untersee Oasis (Lacelle et al., 2024) and in Taylor Valley (B. Lyons et al., 2020). While these past studies focused on two ice free oases, these encrustations also occur on numerous Nunatak surfaces which are the focus of this study.

Here we have selected fourteen carbonate encrustations from the hundreds available collected over a century of Antarctic field work and curated in the Polar Rock Repository (PRR), hosted by The Ohio State University. These fourteen encrustations are from eight locations spanning an area from West Antarctica to the Ross Sea Sector of the Transantarctic Mountains, an area hereon called the Ross Sea Sector (RSS) (Figure 1, Figure 2). This RSS is characterized by average temperatures

well below freezing as shown by over a decade of data collection at Antarctic Weather Stations (AWS). The Janet AWS at 2085m in the interior of West Antarctica has recorded a maximum temperature of -2°C and a minimum of -63.8°C (Antarctic Meteorological Research and Data Center, 2026). The Bear AWS at 416m on the coast of West Antarctica recorded a maximum temperature of 5°C and a minimum of -42.4°C (Antarctic Meteorological Research and Data Center, 2023). As with Arctic samples, their occurrence implies the presence of past surface waters with the important distinction that in most cases these Antarctic samples formed under colder, higher latitude, higher elevation, more extreme conditions than their Arctic counterparts (Environment and Climate Change Canada, 2025; Lacelle, 2007; Lacelle et al., 2007).

Modern surface melting currently occurs in Antarctica during austral summers at low elevations and in coastal regions (Tedesco & Monaghan, 2009; Zheng et al., 2025). Expanded surface melting has been documented using remote sensing techniques and are interpreted to be driven by atmospheric rivers (ARs) which are warm, moisture rich storm events (Maclennan et al., 2023; Wille et al., 2019). Such events may have driven past surface melting during periods of strong El Niño events which correlate with a negative phase of the southern annual mode (SAM) (Nicolas et al., 2017; Scott et al., 2019). These events have also been suggested to increase in frequency with periods of weakening of the Atlantic meridional overturning circulation (AMOC) (Böhm et al., 2015; Scott et al., 2019). Thus any pattern of past surface melting could coincide with the Antarctic Isotope Maximums (AIMs), the

consequence of Southern Ocean warming and AMOC stoppage recorded in ice cores (Barker et al., 2011). While ARs may play a role under the modern warm climate, a list of past surface melting mechanisms includes Earth's orbital variations, global temperature changes (e.g. CO_2), and fluctuations in marine water influence which can vary with the extent of Antarctic ice shelves. In one example, the increase in melt layer frequency in West Antarctica's Siple Dome Ice Core has been interpreted as partly driven by increased proximity to marine waters as the Ross Ice Shelf retreats in the late Holocene (Das & Alley, 2008). Examples of orbitally driven temperature variations include the interpretations of isotopic proxies for temperature in the West Antarctic Ice Sheet Divide Ice Core (WAIS Divide Project Members, 2013). In these cores, local deviations from global climate have been interpreted to reflect a role of Southern Hemisphere summer insolation (SHSI) (WAIS Divide Project Members, 2013) or possibly Southern Hemisphere summer duration (Huybers & Denton, 2008).

Currently, geologic records of past surface melting are few. Ice rafted debris in ocean sediment cores record large scale ice loss to the Southern Ocean (Jasper et al., 2024; McKay et al., 2022), but do not provide insight into incipient surface melting; and ice core melt frequency records are limited to lower elevations and restricted to the Holocene and latest Pleistocene (Das & Alley, 2008). Given the limited understanding of modern Antarctic surface melting and the extremely few records of surface melting in the past, a different means of identifying past surface melting would be useful to understand past and future surface mass balance in Antarctica. The ability to date the timing of past surface melting at a wide range of

geographic locations and elevations, would provide the possibility that any temporal pattern in their formation allows evaluation of possible climatic drivers. Here we work to determine if the RSS Antarctic carbonate crusts share a formation mechanism with the previously studied Arctic and Antarctic occurrences. This includes testing whether these Antarctic crusts formed from surface waters and determining the process by which this surface melting occurs. Specifically, this requires us to identify the source of salts—which we determine using strontium isotopic analyses—and to test whether they form via evaporation–which we determine using oxygen and carbon isotopic analyses. These oxygen isotope results can also be used to place limits on the isotopic composition of the parent surface meltwater. Finally, we look to evaluate if these crusts can be dated by U-Th disequilibrium methods. While this geochronologic method has not been applied to date Arctic or Antarctic crusts, it has been successfully employed to date pedogenic carbonates and calcite encrustations from deserts (Zamanian et al., 2016).

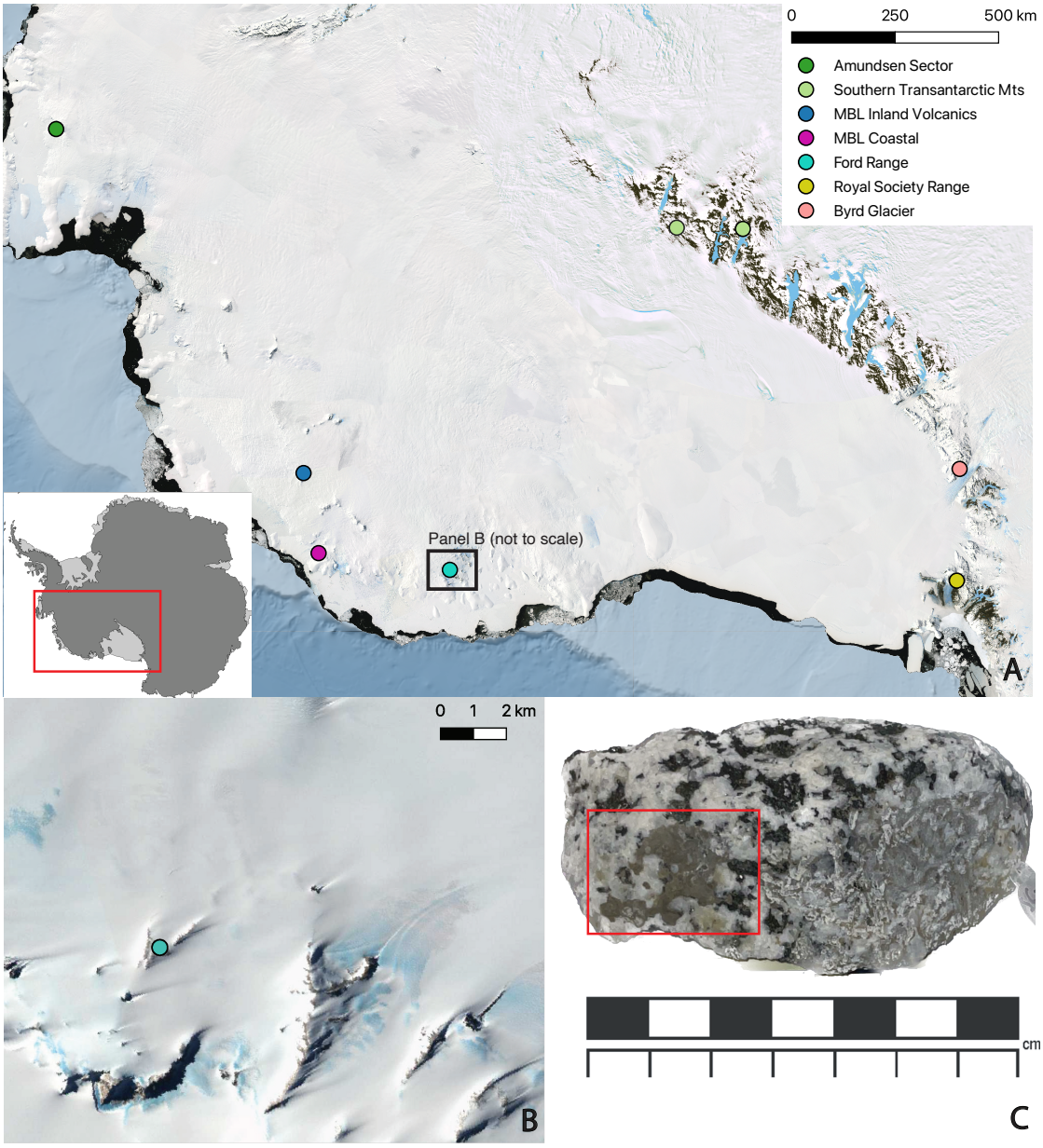

Figure 1. (A) Regional map of the Ross Sea Sector of Antarctica with each sample location indicated by a colored dot. The inset shows the map location in Antarctic. Red outline on the inset of the Antarctic Continent shows the Ross Sea Sector. (B) Satellite image of the Ford Ranges with cyan dot marking the sample location. (C) Photo of a sample (SC_C4) from the Ford Ranges on a host rock of Granodiorite. The red box outlines the area with carbonate appearing brown-gray. The carbonate on the right side has been removed for measurement. Basemap and imagery created using the QAntarctica package (Matsuoka et al., 2021).

Figure 2. (A) Photo of sample PRR_33067. The host rock is basalt, and the red outline shows one of the sampling locations.

2. Materials and Methods

2.1 U-Th Isotopic Data

We used ^{234}U-^{230}Th methods to determine the time of formation for each carbonate. These ^{234}U-^{230}Th isotopic data were collected on the UCSC IsotopX X62 Thermal Ionization Mass Spectrometer (TIMS) using methods modified from Piccione et al., (2022), for applications to these thin carbonate crusts. First, a fine bit Dremel is used to carefully isolate the carbonate coating from the host rock. Any host rock that is accidentally ground off is extracted with tweezers. The amount of powdered carbonate used for each measurement varies from 10mg to 200mg depending on carbonate abundance and uranium concentration. The calcite is dissolved in 7N nitric acid and spiked with a ^{236}U-^{229}Th tracer. Uranium and thorium are isolated using an AG-1X resin. Then, the uranium and thorium are loaded onto

filaments and measured on the UCSC IsotopX X62 Thermal Ionization Mass Spectrometer (TIMS).

U-Th disequilibrium ages assume that parent ^{234}U was fractionated from intermediate daughter ^{230}Th due to the contrast in water solubilities (U soluble, Th insoluble). However, it is common for a pedogenic carbonate to exhibit elevated thorium concentrations, perhaps due to the weathering and evaporation of a thin film of water that forces the incorporation of this otherwise insoluble element. The degree to which initial (detrital) thorium was incorporated was determined by measuring ^{232}Th, as it is not a part of the ^{238}U decay chain. Because young samples have low ^{230}Th accumulation via radioactive decay of ^{234}U, a detrital ^{230}Th correction is crucial. We corrected for the detrital ^{230}Th by measuring the detrital ^{232}Th and the naturally occurring relative abundances. Samples with abundant detrital thorium have low $[^{230}Th/^{232}Th]$ (where brackets denote activity ratios). We constructed isochrons (Osmond et al., 1970; Rosholt, 1976; Vermeesch, 2018) to simultaneously correct for detrital thorium and calculate an age. Isochron construction required more than one measurement of each sample (Figure 3).

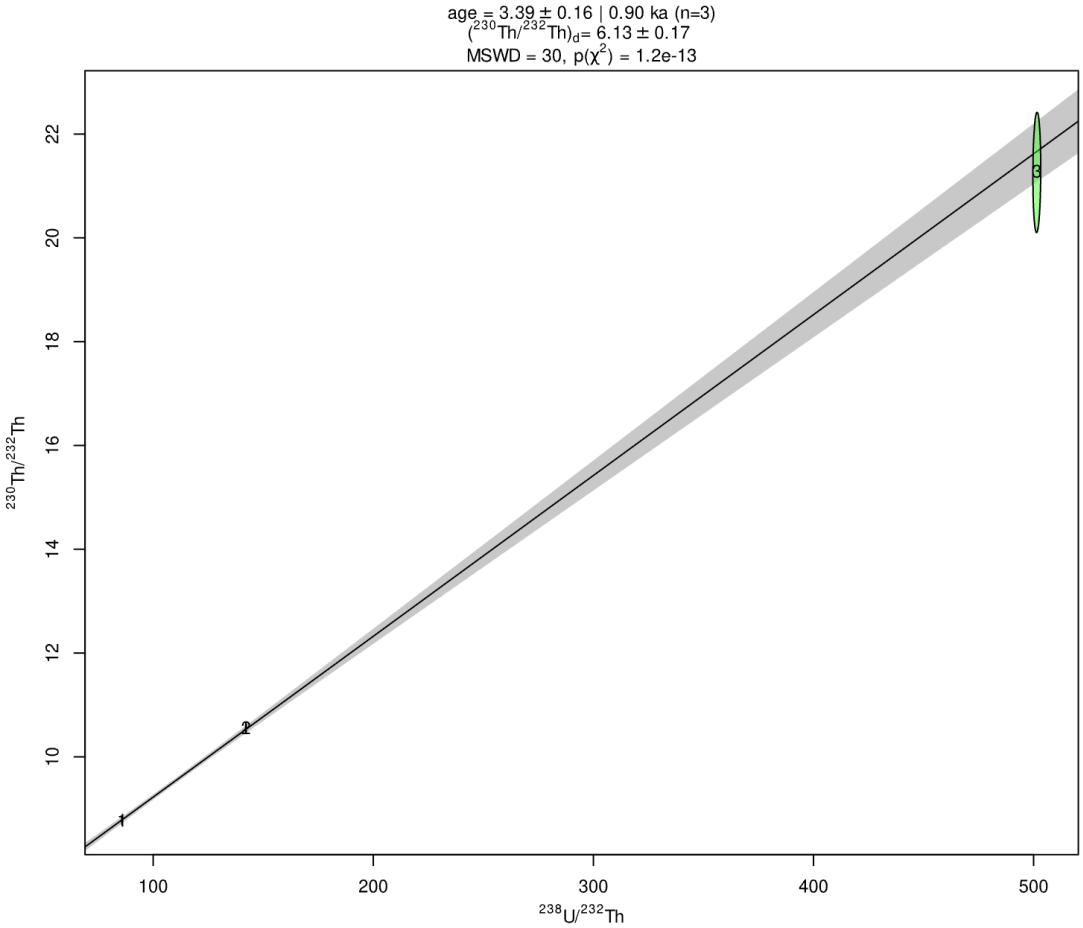

Figure 3. Rosholt A Isochron with three measurements for PRR_33067. Age: 3.39 ± 0.16 ka. Age uncertainty: 4.7%.

2.2 Carbon, Oxygen, and Strontium Isotopic Data

Carbonate isotope ratios ($\delta^{13}C$ and $\delta^{18}O$) were measured by the UCSC Stable Isotope Laboratory using a Themo Scientific Kiel IV carbonate device and MAT 253 isotope ratio mass spectrometer. An aliquot of the same powdered carbonate used for the ^{234}U-^{230}Th age measurement was used for $\delta^{13}C$ and $\delta^{18}O$ measurements.

Measurements of the $^{87}Sr/^{86}Sr$ isotopic composition were performed on the same sample volume used to measure U-Th isotopic compositions using the Sr eluted

during U-Th purification. A dilute nitric acid (7N) was used to avoid dissolution of any silicate minerals from the host rock that were unintentionally incorporated while isolating the carbonate crust with a Dremel. These Sr "washes" were purified using a Sr-spec AG-1X resin. The Sr was measured on the UCSC IsotopX X62 TIMS in a three-sequence static measurement. Accuracy of the $^{87}Sr/^{86}Sr$ measurements is evaluated using Sr standard SRM987 compared to a long-term laboratory average value of 0.71024, with a typical reproducibility of ±0.00004.

3. Results

Of the fourteen carbonates used in this study, ^{234}U-^{230}Th ages range from 2.0ka (thousand years ago) to 99.5ka with percent uncertainties that range from 1.8% to 107.7% (Table 1). Eleven of these ages are <10ka and cluster between 2ka and 6ka. The three older carbonates are East Antarctic samples from high elevation (over 1400m) field sites with the ages 43.04ka ± 3.27ka (PRR12678), 92.9ka ± 2.3ka (PRR36401), and 97.8ka ± 4.7ka (PRR36574). The [$^{234}U/^{238}U$] (where brackets denote Activity ratios) of each carbonate range from 0.89 to 1.74. The uranium concentrations range from 0.1ppm to 302.3ppm. The [$^{230}Th/^{232}Th$] is low for most samples and ranges from 0.52 to 22.09; the [$^{230}Th/^{232}Th$] of all but four samples, three of which are from the Holocene, are less than 7 (Table 1).

The carbon and oxygen measurements of each sample yield compositions that range from ~6 to 14‰ $\delta^{13}C_{VDPB}$ and ~-12 to -5‰ $\delta^{18}O_{VDPB}$ (Table 2). The carbon and oxygen isotope values show a positive correlation with each other.

The strontium composition varies over a wide range across the combined dataset of all the samples, with $^{87}Sr/^{86}Sr$ values between 0.70418 ± 0.00063 and 0.72537 ± 0.00083 (Table 2). In general, the $^{87}Sr/^{86}Sr$ value of each carbonate crust is related to the clast that the crust is coating (host rock). The lowest $^{87}Sr/^{86}Sr$ value is from a crust on a basalt host rock while the two highest $^{87}Sr/^{86}Sr$ values are both crusts on gneiss host rocks (Table 2).

Sample Run/ID	[Th] (ppm)	[U] (ppm)	[232Th / 238U]	+/-2s (%)	[230Th / 232Th]*	+/-2s (%)	[230Th / 238U]	+/-2s (%)	[234U / 238U]	+/-2s (%)	U-Th age (ka)	+/-2s (ka)	U-Th age (Th corr.) (ka)**	+/-2s (ka)	[234U / 238U]	+/-2s
SC_B7_1_1	10.87	63.97	0.0554	1.81	1.63	10.17	0.0904	10.33	1.0602	0.60	9.72	1.05	4.93	2.60	1.062	0.0065
SC_B7_3_1	11.01	56.25	0.0639	0.26	1.35	2.48	0.0865	2.49	1.1359	0.13	8.62	0.22	3.48	2.57	1.139	0.0015
SC_B7_4_1	11.39	39.96	0.0930	0.22	1.25	1.20	0.1164	1.22	1.0699	0.21	12.55	0.16	2.63	3.52	1.072	0.0023
SC_C4_1	2.60	281.56	0.0030	0.87	22.09	1.39	0.0665	1.64	1.0468	0.12	7.16	0.12	6.90	0.17	1.048	0.0013
SC_C4_2	1.80	302.30	0.0019	0.34	21.53	1.35	0.0417	1.39	1.0196	0.13	4.55	0.06	4.38	0.11	1.020	0.0014
SC_E3_1	32.68	88.88	0.1199	0.44	1.07	2.38	0.1283	2.42	1.2196	0.81	12.08	0.33	2.93	4.68	1.227	0.0102
SC_E3_2	12.65	34.76	0.1187	0.09	1.13	1.83	0.1336	1.83	1.2892	0.24	11.89	0.23	3.34	4.33	1.299	0.0032
SC_E3_3_1	10.94	36.21	0.0986	0.14	1.15	3.16	0.1130	3.16	1.2441	0.13	10.35	0.34	3.04	3.70	1.251	0.0016
PRR_33067_3_1	4.90	137.25	0.0116	0.09	8.77	0.74	0.1022	0.75	0.9999	0.14	11.76	0.09	7.88	0.20	1.000	0.0014
PRR_33067_5_1	3.33	154.27	0.0070	0.08	10.55	0.80	0.0743	0.80	0.9965	0.21	8.44	0.07	7.67	0.17	0.996	0.0022
PRR_33067_5_2	1.55	253.24	0.0020	0.29	21.26	4.37	0.0424	4.38	1.0114	0.13	4.67	0.21	4.45	0.21	1.012	0.0013
PRR56408_1_2	0.28	2.34	0.0391	0.25	2.38	10.45	0.0931	10.45	1.4013	5.25	7.48	0.91	4.97	1.51	1.410	0.0747
PRR_56408_5_1	0.29	3.31	0.0287	0.09	2.64	4.58	0.0758	4.59	1.3457	0.19	6.31	0.30	3.96	0.56	1.352	0.0026
PRR58295_1	0.25	2.85	0.0282	0.40	2.51	5.03	0.0708	5.05	1.1068	2.50	7.21	0.42	4.90	1.20	1.109	0.0282
PRR_58295_3_1	0.20	3.12	0.0212	0.10	2.98	8.15	0.0631	8.15	1.0902	0.25	6.50	0.54	4.75	1.02	1.092	0.0028
PRR_58295_5_1	0.33	3.04	0.0357	0.21	2.01	12.29	0.0718	12.29	1.0823	0.37	7.48	0.95	3.83	1.21	1.084	0.0041
PRR4622_1	0.73	15.27	0.0156	0.29	3.71	5.88	0.0580	5.89	1.1043	0.36	5.88	0.36	4.60	0.72	1.106	0.0040
PRR4622_2	0.04	1.35	0.0086	0.17	7.25	1.77	0.0627	1.78	1.0977	0.11	6.41	0.12	5.70	0.37	1.099	0.0012
PRR4624_1	0.90	22.77	0.0128	0.12	3.43	1.57	0.0440	1.57	1.1055	0.38	4.43	0.07	3.38	0.52	1.107	0.0042
PRR4624_2	1.17	17.94	0.0214	0.27	2.46	3.64	0.0526	3.65	1.1089	0.26	5.30	0.20	3.56	0.87	1.111	0.0029
PRR_4624_3_1	0.98	16.95	0.0188	0.10	2.43	4.89	0.0456	4.89	1.1108	0.59	4.57	0.23	3.05	0.78	1.112	0.0066
PRR_4601_6_1	14.42	9.81	0.4799	0.36	0.95	2.25	0.4566	2.28	1.0507	0.15	61.85	1.89	10.83	28.41	1.060	0.0018
PRR_4601_6_2	3.19	12.62	0.0824	0.22	1.36	2.29	0.1120	2.30	1.1163	4.19	11.51	0.59	4.71	3.45	1.120	0.0482
PRR4601_1_1	1.42	7.47	0.0619	0.55	1.52	8.42	0.0938	8.44	1.1114	0.12	9.60	0.84	4.51	2.69	1.114	0.0014
PRR_36401_6_1	0.21	1.15	0.0610	0.10	8.38	0.92	0.5107	0.93	0.8886	0.48	95.61	1.69	89.03	3.69	0.854	0.0060
PRR_36401_6_2	0.71	9.23	0.0252	0.06	21.92	0.92	0.5521	0.92	0.9392	0.16	97.97	1.51	95.48	2.98	0.920	0.0021
PRR_12678_6_1	6.07	1.26	1.5700	0.74	0.52	18.66	0.8177	18.67	1.5544	0.35	77.62	20.15	11.42	99.63	1.690	0.0399
PRR12678_2	0.50	0.35	0.4669	0.97	1.22	1.87	0.5688	2.11	1.5802	0.38	47.25	1.23	17.79	16.81	1.663	0.0067
PRR12678_3	0.36	0.10	1.1328	1.80	0.55	5.66	0.6284	5.94	1.5782	0.67	53.53	4.00	-8.50	15.07	1.672	0.0136
PRR36574_1_1	0.18	1.20	0.0502	2.63	14.90	1.74	0.7476	3.15	1.1469	2.88	111.56	8.56	107.73	8.72	1.201	0.0420
PRR36574_1_2	0.21	1.28	0.0531	0.42	15.08	1.48	0.8016	1.54	1.1641	0.73	122.13	3.81	118.20	4.27	1.232	0.0111
PRR36574_1_3	0.17	0.87	0.0649	0.60	12.48	0.76	0.8106	0.97	1.1392	0.68	130.35	3.03	125.40	3.90	1.201	0.0102
PRR36574_1_4	0.72	1.17	0.2022	2.56	5.14	1.51	1.0385	2.97	1.1583	2.49	220.74	28.49	205.60	29.43	1.295	0.0404
PRR36714_1_1	0.95	2.35	0.1318	0.18	3.04	2.24	0.4014	2.25	1.0728	0.23	50.80	1.45	39.28	6.08	1.084	0.0028
PRR36714_1_2	1.08	2.57	0.1375	1.47	2.86	1.86	0.3930	2.37	1.1373	3.95	45.84	2.71	34.57	6.24	1.156	0.0500
PRR36714_1_3	1.06	1.78	0.1942	0.49	2.84	2.33	0.5523	2.38	1.0782	0.26	77.45	2.67	60.21	9.49	1.097	0.0034
PRR37868_1_1	0.31	1.95	0.0518	6.34	2.34	17.52	0.1209	18.63	1.6917	1.16	8.05	1.55	5.30	2.08	1.708	0.0202
PRR37868_1_2	0.34	1.95	0.0574	1.10	1.77	2.65	0.1013	2.87	1.7354	0.71	6.53	0.20	3.55	1.49	1.749	0.0125
PRR37868_1_4	0.96	2.08	0.1503	0.76	1.41	5.90	0.2115	5.95	1.6975	0.25	14.39	0.91	6.25	4.24	1.726	0.0047

Table 1. Summary of U-Th isotopic data. * For samples with a $^{230}Th/^{232}Th > 20$, the detrital thorium quantity is low enough that we did not need to do an isochron. ** For

samples that did not need an isochron, an average of the values in the "U-Th age (Th corr.) (ka)" column are used as ages for this study.

Sample Run/ID	Location	Elevation (m)	Host Rock Type	δ13C	δ18O	87Sr/86Sr	abs std error (2 sigma)
PRR33067	Amundsen Sector	1204	basalt	11.42	-6.77	7.112E-01	1.319E-05
				10.33	-6.7	7.114E-01	1.529E-05
				11.25	-6.07		
PRR56408	MBL Inland Volcanics	2560	basalt/dacite	7.05	-11.48	7.083E-01	1.226E-05
				6.84	-10.94		
PRR58295	MBL Coastal	366	basalt	8.22	-6.7	7.042E-01	1.259E-05
				8.39	-6.91		
				8.47	-6.55		
SC_B7	Ford Range	1025	kspar-granite	10.79	-5.87	7.087E-01	1.313E-05
				10.49	-6.74		
				12.6	-5.67		
				10.62	-4.54		
SC_C4	Ford Range	1025	granodiorite	10.62	-7.87	7.112E-01	1.432E-05
				10.94	-9.06	7.127E-01	1.420E-05
				8.77	-10.43		
				6.9	-12.44		
SC_E3	Ford Range	1025	rhyolite	13.99	-5.18	7.085E-01	1.255E-05
				14.15	-5.3	7.079E-01	1.372E-05
				14.19	-5.78		
PRR4622	Royal Society Range	868	gneiss	8.93	-9.97	7.254E-01	1.658E-05
				9.98	-10.77		
				8.72	-10.6		
PRR4624	Royal Society Range	868	basalt	10.74	-5.76	7.101E-01	1.180E-05
				8.71	-7.66		
				9.45	-7.47		
PRR4601	Royal Society Range	415	gneiss	7.34	-9.41	7.193E-01	7.867E-05
PRR37868	S. Transantarctic Mtns	789	basalt	11.449	-9.62		
				11.848	-9.89		
PRR12678	S. Transantarctic Mtns	2500	sandstone	8.47	-8.06		
				5.92	-10.64		
PRR36714	Byrd Glacier	1405	limestone	10.56	-11.61		
				10.13	-11.30		
PRR36574	Byrd Glacier	1996	limestone	8.94	-10.52		
				9.07	-11.10		
PRR36401	Byrd Glacier	1387	limestone	11.53	-10.09		
				7.54	-10.18		

Table 2. Summary of carbon, oxygen, and strontium isotopic data, and other relevant sample information. Carbon and oxygen measurements are in VPBD. Duplicate lines are shown for samples with multiple measurements.

4. Discussion

4.1 Constraints from Carbon and Oxygen Data

The carbon and oxygen isotopic measurements from these Antarctic evaporitic carbonates yield relatively high compositions from 6 to 14‰ $\delta^{13}C_{VDPB}$ and -13 to -5‰ $\delta^{18}O_{VDPB}$ (Figure 4). The carbon compositions are up to 10‰ higher than the

highest possible source of carbon (+5 ‰, carbonate rocks). The oxygen compositions, converted to water $\delta^{18}O_{SMOW}$ compositions are between -15 and -23‰, (assuming equilibrium formation with air temperatures of -30 °C), which are higher than Antarctic glacial ice compositions ($\delta^{18}O$ < -30‰) by up to 15‰ and exceed modern coastal precipitation ($\delta^{18}O$ < -20‰) by slightly less (Gasson et al., 2016; Masson-Delmotte et al., 2008). Note that the assumption of -30°C presents an extreme case as warmer temperatures associated with melting of ice or snow yield even higher carbon and oxygen isotope values, further separating the inferred water compositions from ice compositions. In addition to these anomalously high values, the carbon and oxygen compositions are positively correlated, such that the highest carbon values correspond to the highest oxygen values. Both the absolute values, as well as the correlation between these metrics has been interpreted to result from non-equilibrium fractionation during water evaporation (Lacelle, 2007). The magnitude of fractionation has also been interpreted and experimentally shown to correspond with the rate of evaporation (Lacelle, 2007). These carbon and oxygen isotope results also help rule out the alternative case, where freezing drives carbonate formation, as kinetic fractionation during freezing would drive carbonate-water fractionation factors of oxygen lower (Lacelle, 2007), resulting in unrealistically high parent water oxygen isotope values. Thus, we interpret from these results that these carbonates precipitate from waters that form during melting of local snow or ice and subsequent evaporation of surface meltwater.

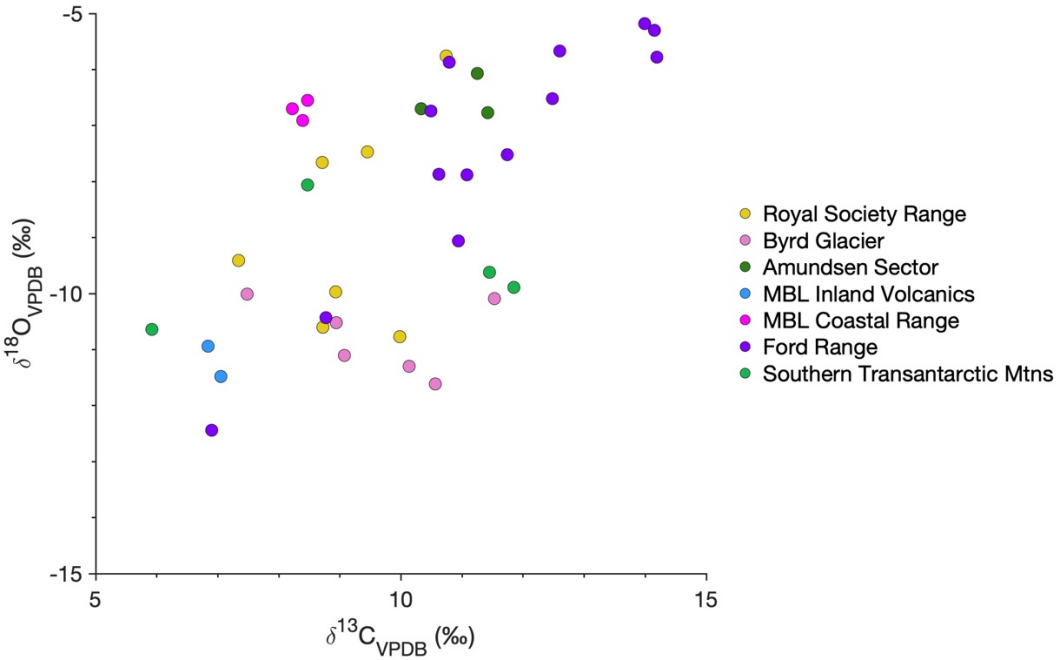

Figure 4. Carbon ($\delta^{13}C$) and oxygen ($\delta^{18}O$) compositions for carbonates in VPBD.

4.2 Constraints from Strontium Isotopic Data

We utilize the $^{87}Sr/^{86}Sr$ composition of each sample to determine the source of the solutes (primarily Ca, which we approximate with Sr) involved in carbonate precipitation (Lyons et al., 2020). Table 2 summarizes the results of $^{87}Sr/^{86}Sr$ measurements. There is high variability in the $^{87}Sr/^{86}Sr$ compositions, even within a single field location. In general, the $^{87}Sr/^{86}Sr$ values of each carbonate crust relates to the host rock they formed upon, which is consistent with the idea that solutes are sourced from local rocks. The carbonates in this study formed on a range of rock types, the lowest $^{87}Sr/^{86}Sr$ values (0.7042) are crusts on basalt, while the highest $^{87}Sr/^{86}Sr$ values (0.7254) are crusts on gneiss, which are more radiogenic, felsic rocks. Past studies of the $^{87}Sr/^{86}Sr$ composition of rock formations in Antarctica show that

the lowest values are present in alkaline basalt groups such as the McMurdo Group volcanics (0.703-0.704) while higher values are present in more felsic rocks such as the Olympus-Granite Gneiss (0.715-0.722) (Lyons et al., 2002). These results support the interpretation that Sr (and therefore Ca) is sourced from weathering local rocks.

4.3 Timing of Carbonate Formation

The carbonates form on exposed rock surfaces and as determined by oxygen and carbon isotopic results, are the result of meltwater from melting local snow or ice. Mechanisms that could melt local snow or ice include warm air temperature or orbital variations that result in intensification of Southern Hemisphere solar radiation. Figure 5 summarizes the U-Th ages of these carbonates allowing us to evaluate these possible drivers. Most of the RSS carbonates, from West and East Antarctica, formed during the Holocene, particularly the mid-late Holocene (2ka-6ka). The weighted mean of the 11 Holocene samples is 4.85ka ± 0.081ka which coincides with a peak in summer temperature which is interpreted to result from rising SHSI (Jones et al., 2023). In East Antarctica, three samples formed prior to the Holocene with the oldest measured age at 99.5ka ± 4.3ka. Figure 5, Panel a, compares carbonate age to the elevation of sample collection to test if an elevation-temperature gradient controls the age pattern. Using modern AWS temperature measurements as a guide, across this over 2000m range in elevation, during past climatically warm periods or ARs we might expect a similar maximum temperature gradient of 7°C (Antarctic Meteorological Research and Data Center, 2026). Given the abundance of Holocene

samples over a wide elevation range (~365m-2560m), it is unlikely that the elevation-temperature gradient drives surface melting conditions. All pre-Holocene samples are limited to higher elevations, suggesting that their preservation requires ice not reclaiming these surfaces as either the ice sheet decreased in size or as glacial ice incised into valleys, stranding these high elevation surfaces.

To further evaluate whether high polar temperatures drive these surface melting events, we compare the age distribution to polar temperature proxies, specifically the WAIS Divide and Epica Dome C ice core hydrogen isotopic records. Figure 5, Panel b compares carbonate ages (blue boxes) to Antarctic temperature proxies from WDC (black line, Cuffey et al., 2016) and from δD from EDC (blue line, Parrenin et al., 2013). The carbonate ages (Figure 5, blue boxes) in this study formed during both the colder glacial period before the Holocene and during the warmer Holocene. Several carbonate ages fall within glacial intervals (41ka, 93ka, and 99ka), when summer temperatures were substantially lower than during interglacial periods. If mean summer temperature were the primary control on Antarctic surface melting, carbonate formation would be expected to cluster during warm interglacial summers. Instead, the distribution of ages across both warm and cold intervals indicates that atmospheric temperature alone does not control the occurrence of these surface melt events.

Today, surface melting in Antarctica is widely documented during austral summers, particularly at low elevations and in coastal regions (Tedesco & Monaghan, 2009; Wille et al., 2019; Zheng et al., 2025). Most modern surface melting events

coincide with AR events which bring warm, moisture rich air onto the continent (Maclennan et al., 2023). While it is possible that warm AR events provided the conditions for surface melt at the locations of these carbonates, we recognize that these events may not have been able to produce melt at the high elevation or inland sample locations. For example, over a decade of data collection, AWS Janet at 2085m recorded a maximum temperature of -2°C and a minimum of -63.8°C, indicating air temperatures never reached above freezing. Three carbonates in this study formed at a similar elevation, further inland, and at a time, before the Holocene, when average global temperatures were lower than today. These observations suggest that ARs alone cannot explain the timing and spatial distribution of carbonate formation in this study.

We now turn to whether changes in Earth's orbital variations over the timescale of this study control the pattern of carbonate formation. It has long been noted that changes in global and polar climate coincide with changes in Northern Hemisphere summer insolation (NHSI). While it remains unlikely that NHSI directly induces surface melting in the Southern Hemisphere, it has been postulated (Huybers & Denton, 2008) that Antarctic summer duration—which is synchronized with NHSI—could influence surface melting. In Figure 5, Panel c we compare the carbonate ages to July 21 mean daily insolation for 65°N (NHSI) and Southern Hemisphere summer duration (Huybers & Denton, 2008; Laskar et al., 2004). Carbonate ages do not correspond with either of these which decline throughout the Holocene where we see a cluster of carbonate ages. Rather, Figure 5, Panel d shows Dec 21 mean daily

insolation for 75°S (SHSI) (Laskar et al., 2004) where we see a correspondence with carbonate formation ages. This precession dominated signal of SHSI is directly out of phase with NHSI. All carbonates in this study formed at a time when, within 2σ error of carbonate ages, peak SHSI is greater than 540 W/m^2. Therefore, we find it plausible that the meltwater that evaporates and precipitates carbonate results from SHSI passing a threshold above which lower-albedo surfaces on or near nunataks warm up sufficiently for surface melt to occur, even when summer air temperatures overall remain below freezing. We recognize that our current data set includes only three non-Holocene dates, however, they are consistent with the temporal patterns of only one (SHSI) of the proposed climate forcings (Figure 5).

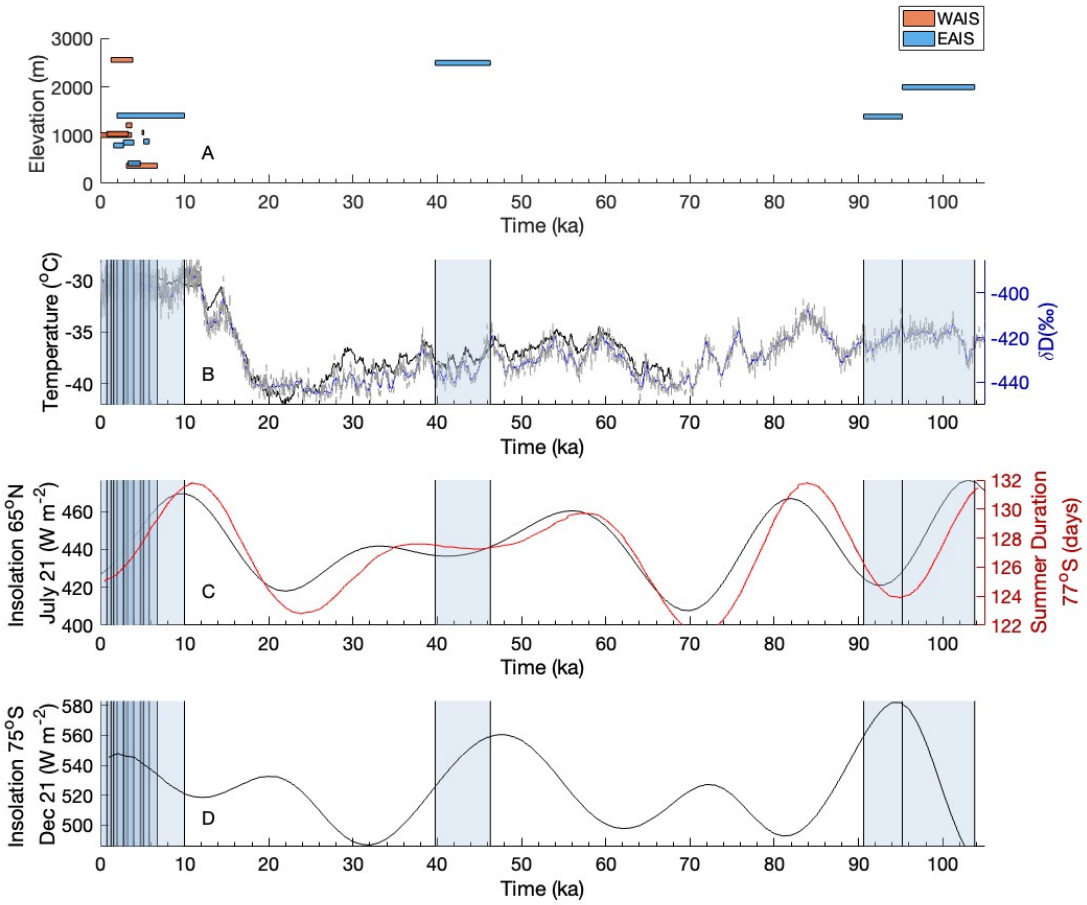

Figure 5. (A) U-Th carbonate ages versus elevation. Horizonal width of markers corresponds to age uncertainty at 2σ. (b-d) Timeseries comparison with U-Th carbonate ages projected on top as blue boxes where horizontal width corresponds to 2σ age uncertainty. (B) Antarctic temperature proxies including (left axis, black) WDC in absolute temperature (Cuffey et al., 2016) which is approximated beyond ~70 ka by visual alignment with the δD from EDC (right axis, blue) (Parrenin et al., 2013). (C) Northern Hemisphere solar forcing including, (left axis, black) July 21 mean daily insolation for 65°N (Laskar et al., 2004) and (right axis, red) summer duration for 77°S as defined by Huybers & Denton, (2008) as the number of days in which the diurnal average insolation intensity exceeds 250 Wm^{-2}. (d) Southern Hemisphere solar forcing for Dec 21 mean daily insolation for 75°S (SHSI) (Laskar et al., 2004).

4.4 Surface Melting Radiative Balance

To illustrate how the local surface energy balance can lead to meltwater production under summer conditions, we use a simple model that assumes the energy budget is dominated by the combination of incoming shortwave solar radiation, outgoing infrared thermal radiation, and the latent heat of melting (when m > 0) or freezing (when m < 0 and sufficient liquid water is present):

$$S(1-\alpha) - \varepsilon\sigma T^4 - mL = 0 \qquad \text{Equation 1a}$$

where S is the solar irradiation per unit surface area (W/m^2), α is the surface albedo (ND), ε is the emissivity (assumed to be 0.97) (Aubry-Wake et al., 2015), σ is the Stefan-Boltzmann constant (ca. 5.67E-8 W/(m^2 K^4)), T is the surface temperature in Kelvin, m is the melting(+) or freezing(-) rate (m/s), and L is the volumetric latent heat of ice fusion (3.06E8 J/m^3). When solved for the melting/freezing rate, this equation becomes:

$$m = \frac{S(1-\alpha) - \sigma T^4}{L} \qquad \text{Equation 1b}$$

For simplicity, our treatment omits turbulent heat fluxes. Van der Broeke et al. (2006) (Van Den Broeke et al., 2006) measured summer turbulent heat fluxes at a high-altitude weather station in Antarctica (their AWS9) and showed that the radiative

budget dominates the surface energy balance, especially on summer days when surface melting is most likely. We justify the simplifications underlying our model by the fact that we are not trying to reproduce specific climatic conditions at a specific location, but rather to illustrate the plausibility of summer surface melting at the ice-marginal locations where our samples were found.

In our calculations, we assume that the modeled surface has a temperature of 273.15K, which is the melting temperature of water ice at standard atmospheric pressure. This assumed temperature is higher than the average summer air temperature in Antarctica, but such warm temperatures must be reached locally for snow/ice melting to occur. This assumption means that infrared surface heat loss is fixed and relatively high in our calculations, so the surface albedo required to reach melting conditions is correspondingly low, about 0.35-0.45, given the range of incoming solar radiation values considered here (about 500-560 W/m2). We consider incoming solar radiation values of 500-560 W/m2 because that is the range of values where we see carbonate formation. This albedo is about half the albedo of a pure snow and ice surface and is consistent with the presence of rock dust and/or larger debris interspersed among the snow and ice, as we would expect at the ice-marginal surface locations where samples have been found(Brock et al., 2000). Figure 6 illustrates that plausible variations in solar shortwave radiation and albedo could lead to climate-driven switches between melting and freezing surface conditions. Our preferred interpretation is that climatic periods of high insolation led to an increased frequency of melting, which may also be enhanced by darkening of snow and ice

surfaces due to debris accumulation and ice crystal metamorphosis (Brock et al., 2000).

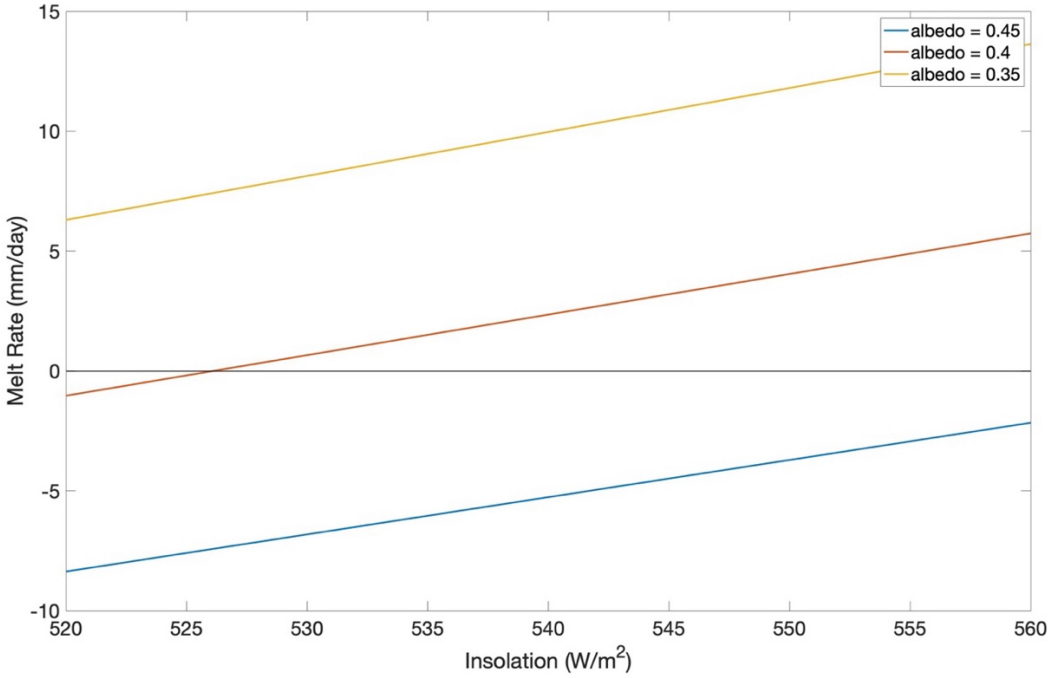

Figure 6. Model results showing insolation versus melt rate for three different albedos. Positive melt rates indicate melting while negative melt rates indicate freezing.

5. Conclusion

The polar environment in various locations in Antarctica has preserved weathered carbonate encrustations on/near lithologically variable nunatak surfaces (Figure 1, Figure 2). Neither local lithology, geographic location, nor elevation controls carbonate formation. The high, positively correlated carbon and oxygen isotopic data indicate carbonate formation through subaerial evaporation (Lacelle, 2007) (Figure 4). The $^{87}Sr/^{86}Sr$ compositions vary over a wide range of values (0.7042 - 0.7254)

even among samples from the same field site. These variations relate to host rock type, suggesting that local meltwater weathers and acquires salts from each cobble (e.g. weathering is in situ). Taken together, these isotopic data support water sourcing from local surface melt, that weathers local rock and saturates carbonate through subaerial evaporation.

The U-Th dating of each carbonate provides the time at which each carbonate precipitated, and therefore, a time when surface melt provided water on a nunatak surface at elevations up to 2500m (Figure 5a). While multiple mechanisms have been proposed to influence Antarctic surface melting including ARs, El Niño–Southern Oscillation variability, shifts in the Southern Annular Mode, CO_2-driven warming, and proximity to marine waters during ice shelf retreat (Freese & Cronin, 2021; Maclennan et al., 2023; Scott et al., 2019; Wille et al., 2019; Zheng et al., 2025), our data are consistent with SHSI forcing among other possibilities. The cluster of late Holocene U-Th dates coincide both with an increase in melt layer frequency at Siple Dome (Das & Alley, 2008) as well as peaks in summer temperatures extracted from the West Antarctic Ice Sheet Divide ice core (Jones et al., 2023), the latter of which has been interpreted to result from rising precession and SHSI through the Holocene (WAIS Divide Project Members, 2013). The older carbonates presented here formed at inland, high elevation locations where marine and AR influence is less likely, and during periods of high SHSI but under colder than modern conditions (Figure 5b). The examined carbonate samples formed during three of the five most recent orbital processional highs that resulted in SHSI values exceeding 540 W/m^2 (Figure 5d).

This comparison between the timing of carbonate formation and SHSI permits estimation of a tipping point in annual maximum summer insolation, of ~540 W/m^2, above which sufficient surface melt occurred at the sample collection sites. A surface radiative balance indicates that these surfaces had an albedo of ~0.4 to yield surface melt (Figure 6). These results are consistent with periods of high SHSI driving an increased frequency of melting on darkened surfaces even while annual average air temperatures remain below freezing. Other forcings may modulate meltwater occurrence over shorter timescales but given the close correspondence of carbonate formation with SHSI highs above the ~540 W/m² threshold, we suggest that insolation provides an important control. This mechanism differs from Arctic carbonate crusts, which also form by evaporation but under warmer conditions where surface water availability is not the deciding factor in the formation of carbonate precipitates (Lacelle et al., 2007).

The coincidence in carbonate formation with time periods marked by high SHSI, supports the role of local radiative heating of lower-albedo surfaces rather than atmospheric temperature changes driving surface melting. The data presented here supports observations (WAIS Divide Project Members, 2013) that local insolation contributes to changes in Antarctic temperature, beyond those produced by CO_2 variations. This surface melt record shows a similar pattern of SHSI driven surface melting but extends the influence of it in both space and time. Our findings may also be relevant to interpretations of Antarctic ice surface histories from cosmogenic

isotopes, which is often based on samples collected in similar environments to those from which our samples were collected.

References

Antarctic Meteorological Research and Data Center. (2023). Bear Peninsula Automatic Weather Station, 2023 quality-controlled observational data. [Text]. AMRDC Data Repository. https://doi.org/10.48567/W8R5-KJ88

Antarctic Meteorological Research and Data Center. (2026). Janet Automatic Weather Station, 2026 quality-controlled observational data. [Text]. AMRDC Data Repository. https://doi.org/10.48567/GWNM-K028

Barker, S., Knorr, G., Edwards, R. L., Parrenin, F., Putnam, A. E., Skinner, L. C., et al. (2011). 800,000 Years of Abrupt Climate Variability.

Böhm, E., Lippold, J., Gutjahr, M., Frank, M., Blaser, P., Antz, B., et al. (2015). Strong and deep Atlantic meridional overturning circulation during the last glacial cycle. *Nature*, *517*(7532), 73–76. https://doi.org/10.1038/nature14059

Brock, B. W., Willis, I. C., & Sharp, M. J. (2000). Measurement and parameterization of albedo variations at Haut Glacier d'Arolla, Switzerland. *Journal of Glaciology*, *46*(155), 675–688. https://doi.org/10.3189/172756500781832675

Cuffey, K. M., Clow, G. D., Steig, E. J., Buizert, C., Fudge, T. J., Koutnik, M., et al. (2016). Deglacial temperature history of West Antarctica. *Proceedings of the National Academy of Sciences*, *113*(50), 14249–14254. https://doi.org/10.1073/pnas.1609132113

Das, S. B., & Alley, R. B. (2008). Rise in frequency of surface melting at Siple Dome through the Holocene: Evidence for increasing marine influence on the climate of West Antarctica. *Journal of Geophysical Research: Atmospheres*, *113*(D2), 2007JD008790. https://doi.org/10.1029/2007JD008790

Environment and Climate Change Canada. (2025, October 15). Canadian Climate Normals - Climate - Environment and Climate Change Canada [G]. Retrieved January 15, 2026, from https://climate.weather.gc.ca/climate_normals/

Freese, L. M., & Cronin, T. W. (2021). Antarctic Radiative and Temperature Responses to a Doubling of CO_2. *Geophysical Research Letters*, *48*(17), e2021GL093676. https://doi.org/10.1029/2021GL093676

Gasson, E., DeConto, R. M., & Pollard, D. (2016). Modeling the oxygen isotope composition of the Antarctic ice sheet and its significance to Pliocene sea level. *Geology*, *44*(10), 827–830. https://doi.org/10.1130/G38104.1

Huybers, P., & Denton, G. (2008). Antarctic temperature at orbital timescales controlled by local summer duration. *Nature Geoscience*, *1*(11), 787–792. https://doi.org/10.1038/ngeo311

Jasper, C. E., Dyer, B., Reilly, B. T., Williams, T., Hemming, S., & Raymo, M. E. (2024). A 3.3-Million-Year Record of Antarctic Iceberg Rafted Debris and Ice Sheet Evolution Quantified by Machine Learning. *Paleoceanography and Paleoclimatology*, *39*(9), e2024PA004897. https://doi.org/10.1029/2024PA004897

Jones, T. R., Cuffey, K. M., Roberts, W. H. G., Markle, B. R., Steig, E. J., Stevens, C. M., et al. (2023). Seasonal temperatures in West Antarctica during the Holocene. *Nature*, *613*(7943), 292–297. https://doi.org/10.1038/s41586-022-05411-8

Lacelle, D. (2007). Environmental setting, (micro)morphologies and stable C–O isotope composition of cold climate carbonate precipitates—a review and evaluation of their potential as paleoclimatic proxies. *Quaternary Science Reviews*, *26*(11–12), 1670–1689. https://doi.org/10.1016/j.quascirev.2007.03.011

Lacelle, D., Lauriol, B., & Clark, I. D. (2007). Origin, age, and paleoenvironmental significance of carbonate precipitates from a granitic environment, Akshayuk Pass, southern Baffin Island, Canada. *Canadian Journal of Earth Sciences*, *44*(1), 61–79. https://doi.org/10.1139/e06-088

Lacelle, D., Christy, M., Faucher, B., Sobron, P., & Andersen, D. (2024). Palaeo-environmental significance of evaporative calcite crusts in the Untersee Oasis, East Antarctica. *Antarctic Science*, *36*(3), 149–159. https://doi.org/10.1017/S0954102024000075

Laskar, J., Robutel, P., Joutel, F., Gastineau, M., Correia, A. C. M., & Levrard, B. (2004). A long-term numerical solution for the insolation quantities of the Earth. *Astronomy & Astrophysics*, *428*(1), 261–285. https://doi.org/10.1051/0004-6361:20041335

Lyons, B., Foley, K., Carey, A., Diaz, M., Bowen, G., & Cerling, T. (2020). The isotopic geochemistry of CaCO3 encrustations in Taylor Valley, Antarctica: Implications for their origin. *Acta Geographica Slovenica*, *60*(2), 125–139. https://doi.org/10.3986/AGS.7233

Lyons, W. B., Nezat, C. A., Benson, L. V., Bullen, T. D., Graham, E. Y., Kidd, J., et al. (2002). Strontium Isotopic Signatures of the Streams and Lakes of Taylor Valley, Southern Victoria Land, Antarctica: Chemical Weathering in a Polar Climate. *Aquatic Geochemistry*, *8*(2), 75–95. https://doi.org/10.1023/A:1021339622515

Maclennan, M. L., Lenaerts, J. T. M., Shields, C. A., Hoffman, A. O., Wever, N., Thompson-Munson, M., et al. (2023). Climatology and surface impacts of atmospheric rivers on West Antarctica. *The Cryosphere*, *17*(2), 865–881. https://doi.org/10.5194/tc-17-865-2023

Masson-Delmotte, V., Hou, S., Ekaykin, A., Jouzel, J., Aristarain, A., Bernardo, R. T., et al. (2008). A Review of Antarctic Surface Snow Isotopic Composition: Observations, Atmospheric Circulation, and Isotopic Modeling*. *Journal of Climate*, *21*(13), 3359–3387. https://doi.org/10.1175/2007JCLI2139.1

Matsuoka, K., Skoglund, A., Roth, G., De Pomereu, J., Griffiths, H., Headland, R., et al. (2021). Quantarctica, an integrated mapping environment for Antarctica, the Southern Ocean, and sub-Antarctic islands. *Environmental Modelling & Software*, *140*, 105015. https://doi.org/10.1016/j.envsoft.2021.105015

McKay, R., Albot, O., Dunbar, G. B., Lee, J. I., Lee, M. K., Yoo, K., et al. (2022). A Comparison of Methods for Identifying and Quantifying Ice Rafted Debris on the Antarctic Margin. *Paleoceanography and Paleoclimatology*, *37*(4), e2021PA004404. https://doi.org/10.1029/2021PA004404

Nicolas, J. P., Vogelmann, A. M., Scott, R. C., Wilson, A. B., Cadeddu, M. P., Bromwich, D. H., et al. (2017). January 2016 extensive summer melt in West Antarctica favoured by strong El Niño. *Nature Communications*, *8*(1), 15799. https://doi.org/10.1038/ncomms15799

Osmond, J. K., May, J. P., & Tanner, W. F. (1970). Age of the Cape Kennedy Barrier-and-Lagoon Complex. *Journal of Geophysical Research*, *75*(2), 469–479. https://doi.org/10.1029/jb075i002p00469

Parrenin, F., Masson-Delmotte, V., Köhler, P., Raynaud, D., Paillard, D., Schwander, J., et al. (2013). Synchronous Change of Atmospheric CO $_2$ and Antarctic Temperature During the Last Deglacial Warming. *Science*, *339*(6123), 1060–1063. https://doi.org/10.1126/science.1226368

Piccione, G., Blackburn, T., Tulaczyk, S., Rasbury, E. T., Hain, M. P., Ibarra, D. E., et al. (2022). Subglacial precipitates record Antarctic ice sheet response to late Pleistocene millennial climate cycles. *Nature Communications*, *13*(1), 5428. https://doi.org/10.1038/s41467-022-33009-1

Rosholt, J. (1976). 230TH/234U DATING OF TRAVERTINE AND CALICHE RINDS. Retrieved from http://pascal-

francis.inist.fr/vibad/index.php?action=getRecordDetail&idt=PASCALGEODEBRGM7720452730

Scott, R. C., Nicolas, J. P., Bromwich, D. H., Norris, J. R., & Lubin, D. (2019). Meteorological Drivers and Large-Scale Climate Forcing of West Antarctic Surface Melt. *Journal of Climate*, *32*(3), 665–684. https://doi.org/10.1175/JCLI-D-18-0233.1

Tedesco, M., & Monaghan, A. J. (2009). An updated Antarctic melt record through 2009 and its linkages to high-latitude and tropical climate variability. *Geophysical Research Letters*, *36*(18), 2009GL039186. https://doi.org/10.1029/2009GL039186

Vermeesch, P. (2018). IsoplotR: A free and open toolbox for geochronology. *Geoscience Frontiers*, *9*(5), 1479–1493. https://doi.org/10.1016/j.gsf.2018.04.001

WAIS Divide Project Members. (2013). Onset of deglacial warming in West Antarctica driven by local orbital forcing. *Nature*, *500*(7463), 440–444. https://doi.org/10.1038/nature12376

Wille, J. D., Favier, V., Dufour, A., Gorodetskaya, I. V., Turner, J., Agosta, C., & Codron, F. (2019). West Antarctic surface melt triggered by atmospheric rivers. *Nature Geoscience*, *12*(11), 911–916. https://doi.org/10.1038/s41561-019-0460-1

Zamanian, K., Pustovoytov, K., & Kuzyakov, Y. (2016). Pedogenic carbonates: Forms and formation processes. *Earth-Science Reviews*, *157*, 1–17. https://doi.org/10.1016/j.earscirev.2016.03.003

Zheng, L., Shang, X., Van Den Broeke, M. R., Noël, B., Li, X., Fettweis, X., et al. (2025). Rapid increases in satellite-observed ice sheet surface meltwater production. *Nature Climate Change*, *15*(7), 769–774. https://doi.org/10.1038/s41558-025-02364-4